J Electr Eng Technol.2017; 12(5): 1980-1990
http://doi.org/10.5370/JEET.2017.12.5.1980

ISSN(Print) 1975-0102
ISSN(Online) 2093-7423

Optimal Rotor Shape Design of Asymmetrical Multi-Layer IPM Motors to Improve Torque Performance Considering Irreversible Demagnetization

M. S. Mirazimi*, A. Kiyoumarsi† and S. M. Madani*

Abstract – A study on the multi-objective optimization of Interior Permanent-Magnet Synchronous Motors (IPMSMs) with 2, 3, 4 and 5 flux barriers per magnetic pole, based on Genetic Algorithm (GA) is presented by considering the aspect of irreversible demagnetization. Applying the 2004 Toyota Prius single-layer IPMSM as the reference machine, the asymmetrical two-, three-, four- and five-layer rotor models with the same amount of Permanent-Magnets (PMs) is presented to improve the torque characteristics, i.e., reducing the torque pulsation and increasing the average torque. A reduction of the torque pulsations is achieved by adopting different and asymmetrical flux barrier geometries in each magnetic pole of the rotor topology. The demagnetization performance in the PMs is considered as well as the motor performance; and analyzed by using finite element method (FEM) for verification of the optimal solutions.

Keywords: Interior Permanent-Magnet (IPM), Genetic Algorithm (GA), Electromagnetic torque, Asymmetrical multi-layer rotor design, Demagnetization

1. Introduction

The superior performances of IPM machines including high efficiency, high torque density resulting in a minimum weight and size, good overload capability, and a wide constant power operating range; make them appropriate for electric and hybrid vehicle propulsions [1, 2]. The existence of buried PMs in the rotor core of an IPM machine is essential in generating a hybrid torque including magnet torque and reluctance torque. In fact, the magnet torque is generated by the interaction of stator resultant rotating Magneto Motive Force (MMF) and PMs; and the reluctance torque is produced by the anisotropic magnetic rotor structure [3]. The multi-layer rotor structure can be applied instead of single-layer due to improving the rotor magnetic saliency. Moreover, the rotor core equipped with several flux barriers per pole possesses many performance advantages, like enhancing efficiency, extending a high-speed constant power operating range; and improving the power factor over the single-layer rotor design [4]. The arrangement, geometry and the number of rotor flux barriers mainly affect the machine performance in terms of both average and pulsation torques. Consequently, an optimization procedure is often required to determine rotor geometry in a manner that a high and smooth torque is achieved [5, 6]. However, the application of the shape design optimization process on a PM machine for achieving a sinusoidal air-gap flux density and low cogging torque-as the two main factors for low torque pulsations- has negative effect on demagnetization of PMs [7].

The PM machines, especially the ones used in Electric Vehicles (EVs) and Hybrid Electric Vehicles (HEVs), should be designed with considering demagnetization characteristics of PMs for the following main reasons. First, the PMSM as a traction motor has an armature winding with high current density at peak power rating and high energy PMs to produce high torque in overtaking and hill climbing [8]. Thus, high operating temperature of such motors and the high level of MMF from the stator windings as the main two factors, affect the demagnetization property of the magnets. Second, when the PMSMs are used in traction application, they usually operate in field weakening region and higher d-axis currents are needed to control the air-gap flux at high speeds; therefore, the PMs may be at high risk of demagnetization [9]. Moreover, magnet demagnetization results in higher current than the rated current flowing into the stator winding in order to produce the same load torque and as a consequence, increases the thermal level of the operating point [10, 11].

In this paper, the 2004 Toyota Prius single-layer IPMSM is studied as the reference machine, according to which four case studies of IPM machines consisting of asymmetrical patterns of flux barriers are introduced. These IPM machines include double-layer V-type and three-, four- and five-layer flat-type PM layouts. An optimization approach, based on the GA, is implemented on the structures. The optimization process is governed through improving rated torque performance at the load angle related to Maximum Torque

† Corresponding Author: Dept. of Electrical Engineering, Faculty of Engineering, University of Isfahan, Iran. (kiyoumarsi@eng.ui.ac.ir)
* Dept. of Electrical Engineering, Faculty of Engineering, University of Isfahan, Iran.
Received: March16, 2017; Accepted: June 16, 2017

per Ampere (MTPA) operating point. The process satisfies the design target without increasing the amount of magnets as well as preventing them being irreversibly demagnetized at severe conditions of operating temperature and applied d-axis current. According to the above mentioned ideas, this paper is organized as follows: the baseline IPM motor is studied in section 2. In section 3, IPM machines with asymmetrical multi-layer rotor layouts are presented and optimized based on the GA. The FE results on electro-magnetic performance for the presented configurations are compared and discussed in section 4. Finally, section 5 presents the conclusions.

2. FEM Modelling and Assessing the 2004 Toyota Prius for Torque Production

The IPMSM applied in 2004 Toyota Prius hybrid electric vehicle [12] is considered as the reference machine for the purpose of this study. The basic structure of this Prius electric motor consisting of 8 magnetic poles and 48 stator slots with distributed windings is illustrated in Fig. 1. As observed from the figure, the single-layer PM segments are encased in V-shape cavities at each rotor pole. The major dimensions and the specifications of the reference machine are tabulated in Table 1.

By the means of FE simulations, the rated torque is determined when the motor is at rated conditions. For reducing the size of the model and the finite element analysis required time, only one eighth of the machine

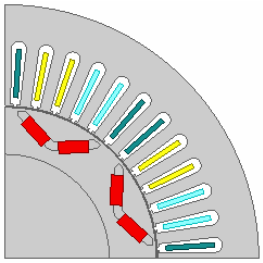

Fig. 1. The structure of the 2004 Prius motor

Table 1. Dimensions and specifications of the 2004 prius motor

Parameter	value
Stator outer/inner radius (mm)	134.6/80.95
Rotor outer/inner radius (mm)	80.2/55.32
Stack length (mm)	83.82
Rated phase current peak value (A)	250
Maximum current (A)	400
Rated speed (rpm)	1500
Rated torque (Nm)	305
Maximum torque (Nm)	400
Iron type	M19-29G
B_r (T) at 50 °C	1.19
H_c (kA/m)	-920
Relative permeability (μ_r)	1.03

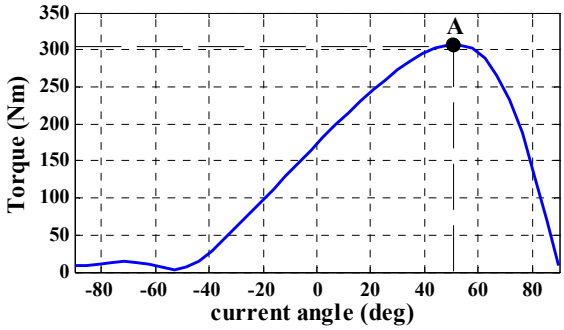

Fig. 2. Torque production of the 2004 Prius motor

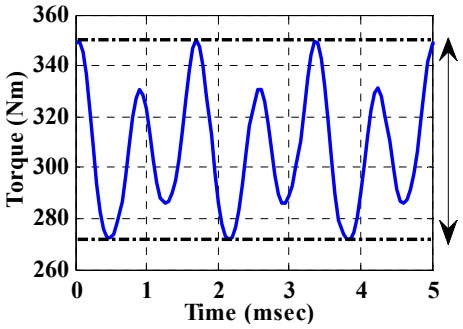

Fig. 3. Electromagnetic torque of the baseline machine at rated conditions

cross section is considered due to its magnetic periodicity characteristic. The output torque of the Prius machine versus the phase angle of the stator current with respect to the q-axis, at rated operating conditions is shown in Fig. 2 (i.e., point A). It is observed that the maximum rated torque of 307.11 Nm can be achieved when the stator current angle is 52.99 electrical degrees. Then, based on this current angle (i.e., point A), the machine is fed and the time-stepping FEM results are shown in Fig. 3. As shown in Fig. 3, the peak-to-peak rated torque is about 26% of the average torque, which are 79.849 Nm and 307.06 Nm, respectively.

3. Parametric Modelling and Optimization Algorithm

The multi-objective optimization problem in this paper is concerned with improving the torque and torque ripple behavior of the multi-layer rotor structures; while, the total volume of PMs used, is the same as the 2004 Prius motor. It should be noted that the demagnetization characteristics of the PMs must be considered as a main design constraint during the optimization. The operating point for the torque determination is chosen to be on the second quadrant of the d-q plane where the machine works along Maximum Torque per Ampere (MTPA) trajectory at rated rotor speed, i.e., Fig. 4. The d– and q–axis currents are determined according to the baseline machine and are kept fixed during

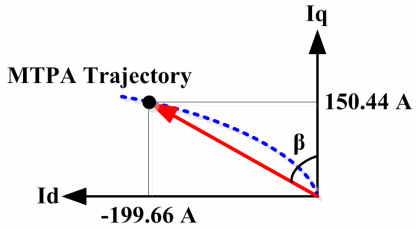

Fig. 4. Current vector in the rated operating point

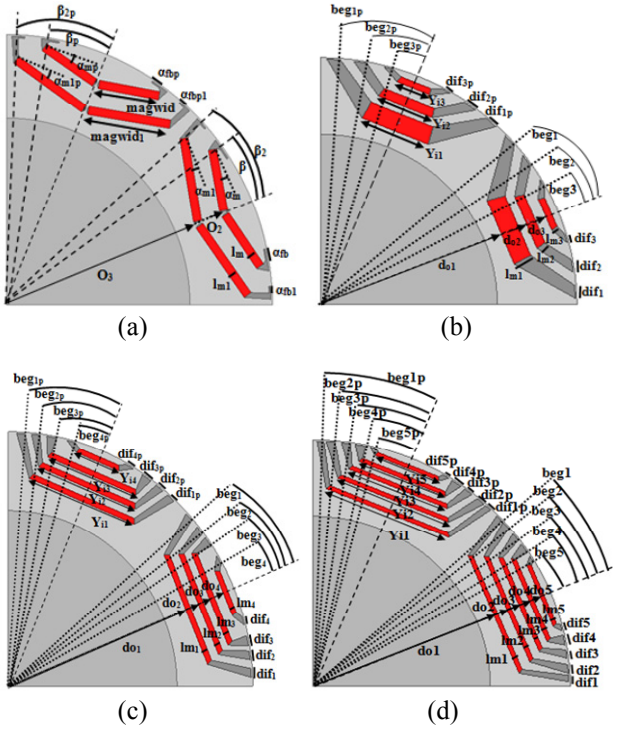

Fig. 5. Parametric model of the optimal: (a) double-layer, (b) three-layer, (c) four-layer and (d) five-layer rotor structures (basic symmetric models)

the optimization process. The current amplitude is chosen according to the thermal considerations. As the stator winding of this Prius uses direct oil-droplet cooling, the nominal current density can reach up to J =15.33 A/mm^2 [13].

3.1 The multi-layer IPM configuration

The parametric modeling of the multi-layer rotor structures (the symmetrical basic models), in which 16, 21, 28 and 35 shape design variables are provided, are illustrated in Figs. 5 (a, b, c and d), respectively.

3.2 Irreversible demagnetization assessment by 2-D FEM

The demagnetization curve of an NdFeB PM (NEOREC35NX) used in 2004 Prius motor is shown in Fig. 6. Irreversible demagnetization test is run to check whether

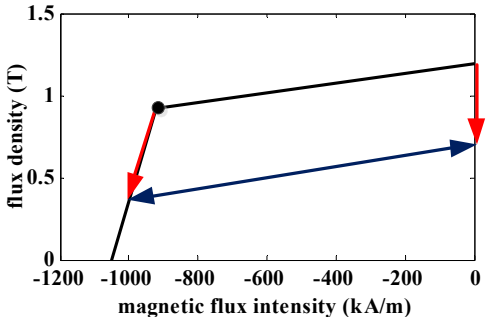

Fig. 6. Demagnetization curve of NEOREC35NX at 180°C

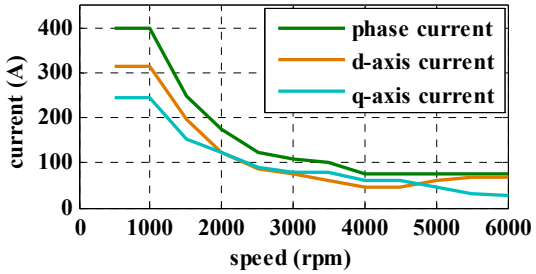

Fig. 7. Input current versus speed for 2004 Prius motor

the optimization process results are trouble free; if so, the results are of concern. The test should be run at 180 °C which is considered as the critical temperature for the PMs used in Prius motor for electric vehicle applications. At this severe temperature, the knee point-where demagnetization occurs-is at the point of 1000 kA/m and 0.92 T (Fig. 6). To evaluate the demagnetization at the severe input current condition, the maximum coercive force in each PM is calculated when the stator current is set to its maximum value, i.e. 400 A and the maximum output torque, i.e. 400 Nm is produced. According to [13], when the 2004 Prius motor operates at the aforementioned conditions, maximum negative direct-axis current value flows in the opposite direction of the PM's MMF (Fig. 7). If the working point of each magnet lies along the identified portion of the curve above the "knee point", it would operate normally and undergoes reversible demagnetization. However, the operation in the area below the knee point, as shown in red in Fig. 6, can cause the magnet to lose some magnetization, irreversibly; since after relaxing the magnetic field intensity the magnet will recoil along a line with lower remanence and the same slope of the original curve, as shown in blue. As a result, if the magnet suffers irreversible demagnetization, the effective B_r drops and the performance of the magnet lowers.

3.3 Optimization based on genetic algorithm

Since several variables are provided for describing the buried PMs and the shape of barriers of the multi-layer rotor structures, and the existence of multiple objective functions-which are in conflict with each other-solving the

Table 2. Design variables and their ranges for five-layer rotor model

Design variables	range	unit	Design variables	range	unit
lm5: magnet width of the fifth layer	1.1~1.6	mm	beg_5/dif_5 : angles of flux barrier of 5th layer at 1st pole	7~9/0.5~2.5	mech.deg
lm4: magnet width of the fourth layer	1.1~1.6	mm	beg_4/dif_4 : angles of flux barrier of 4th layer at 1st pole	9.5~12.5/0.5~2.5	mech.deg
lm3: magnet width of the third layer	1.1~1.6	mm	beg_3/dif_3 : angles of flux barrier of 3rd layer at 1st pole	13~15/0.5~2.5	mech.deg
lm2: magnet width of the second layer	1.1~1.6	mm	beg_2/dif_2 : angles of flux barrier of 2nd layer at 1st pole	16~18/0.5~2.5	mech.deg
lm1: magnet width of the first layer	1.1~1.6	mm	beg_1/dif_1 : angles of flux barrier of 1st layer at 1st pole	18~20/0.5~2.5	mech.deg
Y_{i5}: length of 5th magnet layer	7~11	mm	beg_{5p}/dif_{5p} : angles of flux barrier of 5th layer at 2nd pole	7~9/0.5~2.5	mech.deg
Y_{i4}: length of 4th magnet layer	12~14.2	mm	beg_{4p}/dif_{4p} : angles of flux barrier of 4th layer at 2nd pole	9.5~12.5/0.5~2.5	mech.deg
Y_{i3}: length of 3rd magnet layer	14.5~16.5	mm	beg_{3p}/dif_{3p} : angles of flux barrier of 3rd layer at 2nd pole	13~15/0.5~2.5	mech.deg
Y_{i2}: length of 2nd magnet layer	17~18.2	mm	beg_{2p}/dif_{2p} : angles of flux barrier of 2nd layer at 2nd pole	16~18/0.5~2.5	mech.deg
Y_{i1}: length of 1st magnet layer	18.5~20.5	mm	beg_{1p}/dif_{1p} : angles of flux barrier of 1st layer at 2nd pole	18~20/0.5~2.5	mech.deg
d_{o5}: radial distance of 5th magnet layer	75 ~76.9	mm	d_{o2}: radial distance of 2nd magnet lay	63.496~67.47	mm
d_{o4}: radial distance of 4th magnet layer	71.5~75	mm	d_{o1}: radial distance of 1st magnet layer	57.32~64.296	mm
d_{o3}: radial distance of 3rd magnet layer	67.672~72.6	mm			

design problem is very complicated. As one of the most efficient numerical optimization method-which is widely used in the application of motor design [14]-the GA has been used to carry out the optimization of the proposed multi-layer configurations. The parameters of the GA are set as follows: the population size, mating pool size, individual crossover probability and mutation probability are 20, 20, 1 and 1, respectively.

The design variables, used in the optimization procedure, are shown in Figs. 5 (a, b, c and d). The corresponding variable ranges and limitations are listed in Table 2, for five-layer rotor model, as a vital and final pattern. The data of the other models are also available, but, because of limited space, they are not brought in this paper. The minimum thickness of the PM layers is defined based on the demagnetization analysis as discussed earlier in sub-section 3.2. The limits on the other design variables are chosen to avoid overlapping barriers and unfeasible solutions. Furthermore, consideration of steel center posts near magnets in double-layer rotor topology, as shown in Fig. 5. (a), can improve the mechanical stability. It should be noted that whenever GA reads the output results from the electromagnetic torque obtained through FEM and the volume of the magnets used for each individual, the cost function is calculated by using the weighted values of the individual goal sum square errors, as follows:

$$\begin{aligned} \cos t = & w_1\left(T_{ave} - T_{ave-object}\right)^2 \\ & + w_2\left(T_{pulsation} - T_{pulsation-object}\right)^2 \\ & + w_3\left(V_{PM} - V_{PM-object}\right)^2 \end{aligned} \quad (1)$$

where, the weights w_1, w_2 and w_3 are chosen identically to give the same weight to the electromagnetic torque and volume of the magnets used. It is notable that the optimization process is 'Epsilon-constraint method' which involves minimizing a primary objective torque pulsation, and expressing the other objectives in the form of inequality constraints, as follows:

$$\begin{aligned} & 0 \le T_{pulsation} \le T_{pulsation-object} \\ \text{Constraints: } & -\varepsilon \le V_{PM} - V_{PM-\mathrm{Pr}ius} \le \varepsilon, \\ & T_{ave} \ge T_{ave-object} > 0 \end{aligned} \quad (2)$$

4. Results

4.1 Optimal rotor design of IPM motors

The presented optimization process has been employed to each IPMSM rotor layout. The Flux density contours, which are evaluated by FEA at rated current condition for the optimized rotor structures corresponding to their respective "fittest value" of design variables determined by GA; are illustrated in Fig. 8. It should be noted that the same color scale is used for the sake of comparison. It is evident that the different grades of saturation in the rotor of the five structures are produced in spite of applying the same current loading. It can be said that by increasing the layers of the magnets in the rotor, the iron flux paths around the PMs are more evenly loaded. The plot of the trend of the cost function versus iteration number for optimized five-layer structure, highlighting the optimized design points is illustrated in Fig. 9. It should be noted that, because of limited space, the results for two-, three-, and four-layer machines are not brought in this paper.

The simulation of each model took approximately 15 to 20 minutes, based on the variation of the parameters and the mesh of the model.

4.2 Performance Evaluation of IPM Motors

4.2.1 Average torque results based on the current angle variations

When the rated phase current is applied, the amount of average torque generated by the representative multi-layer structures at various current angles is evaluated by FEM. According to the obtained curves shown in Fig. 10, the maximum rated torque and the corresponding current angle

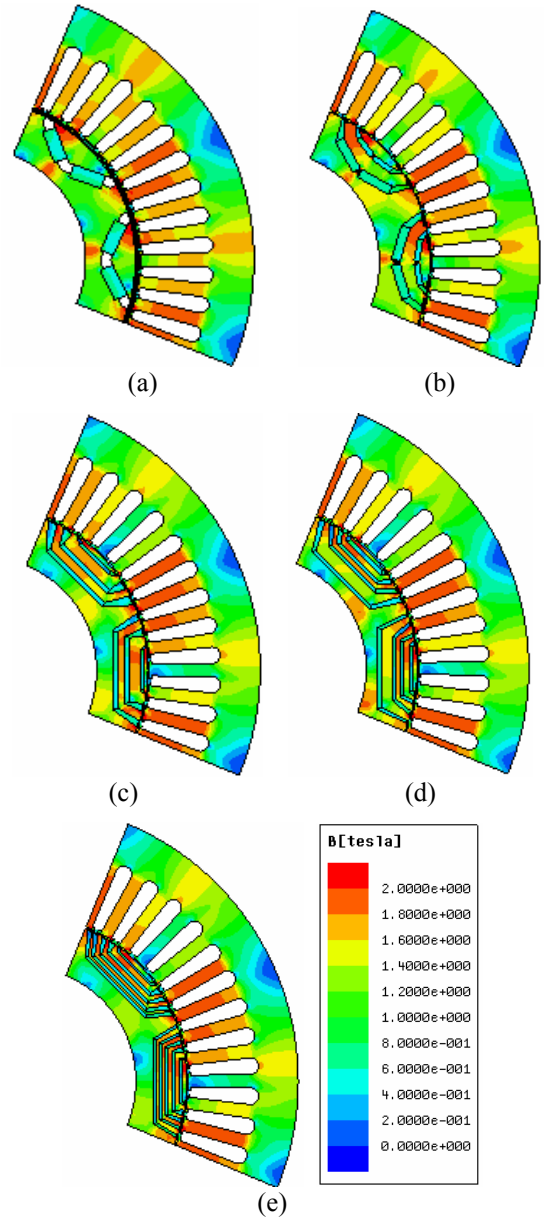

Fig. 8. Flux density contours for the: (a) single-layer, (b) optimal double-layer, (c) optimal three-layer, (d) optimal four-layer and (e) optimal five-layer models at MTPA condition

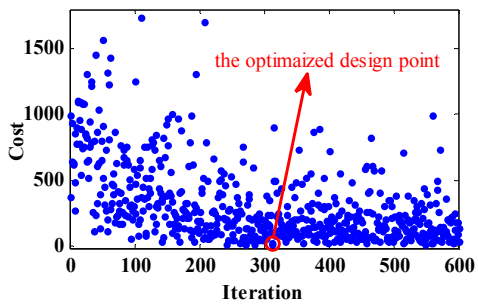

Fig. 9. The trend of cost function for optimized five-layer rotor structure

Table 3. Maximum rated torque and the corresponding current angle for IPM motors

Item	2004 Prius IPM	Two-layer IPM	Three-layer IPM	Four-layer IPM	Five-layer IPM
β	52.9	53.05	53.9	53.2	53.2
$T_{e,max}$	307.11	322.3328	349.5381	348.8941	353.25

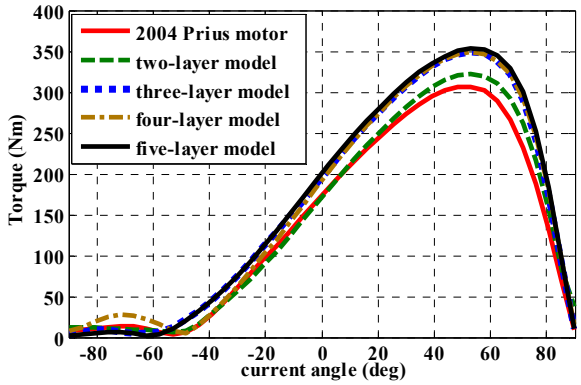

Fig. 10. Torque production of the optimized multi-layer structures

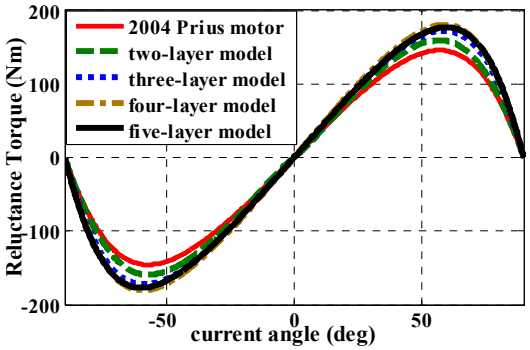

Fig. 11. Reluctance torque production of the optimized multi-layer structures

for each IPM motor are tabulated in Table 3. It can be seen that, with the same amount of magnets as that of the 2004 Prius motor, the amount of rated torque of the proposed double-layer model is increased by 15.2 Nm, i.e., 307.11 Nm is raised to 322.33 Nm. Moreover, in comparison to the reference machine, the amount of rated torque generated by the proposed optimal three-, four- and five-layer models are improved by 42.428 Nm, 41.784 Nm and 46.417 Nm, respectively.

At the rated phase current amplitude of 250 A, the reluctance torque generated by the representative multi-layer optimized structures at various current angles is evaluated by FEM. As the B-H curve of the core permeability is nonlinear in the multi-layer IPM motors with barrier ribs, the reluctance torque is obtained by fixing the core permeability after removing the magnets. The reluctance torque which is shown in Fig. 11 can be expressed in Fourier series expansion as follows:

Table 4. Reluctance torque comparison components (I_a = 250 A)

Item (T_{ek}) (N.m)	2004 Prius IPM	Two-layer IPM	Three-layer IPM	Four-layer IPM	Five-layer IPM
1st component	146.728	154.789	165.651	172.822	169.028
2nd component	29.010	30.975	38.92	41.806	42.404
3rd component	9.576	8.286	12.881	14.069	14.634

Table 5. Rated speed performance comparison of the structures

Item	2004 Prius IPM	Two-layer IPM	Three-layer IPM	Four-layer IPM	Five-layer IPM
PMs(*10^3 mm^3)	138.78	138.723	139.233	138.535	139.881
Rated torque(N.m)	307.11	322.51	349.54	348.93	353.37
Torque pulsation at rated torque (%)	26	10.98	6.4	7.32	6.32
L_d (mH)	1.2068	1.2130	1.1596	1.0542	1.1569
L_q (mH)	2.0515	2.0712	2.0685	2.0598	2.0696
Ψ_{PM} (Wb)	0.1714	0.1857	0.2057	0.1898	0.2084
ζ (saliency)	1.699	1.7075	1.7838	1.9538	1.7889

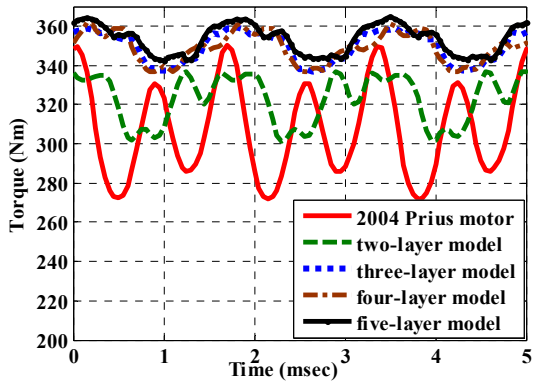

Fig. 12. Electromagnetic torque of all designs at rated condition, i.e., maximum average torque

$$T_e^{\mathrm{Re}luc\tan ce}(\beta) \approx T_{e1}\sin(2\beta+\phi_2)+T_{e2}\sin(4\beta+\phi_4) + \sum_{k=3}^{10} T_{ek}\sin\left((2k\times\beta)+\phi_{2k}\right) > 0 \quad (3)$$

where k is the harmonic order, T_{ek} is Fourier coefficient, Φ_{2k} is the phase angle of the harmonic components and β is the spatial angle of the stator current vector measured with respect to the q-axis.

The decomposed reluctance torque components for the 2004 Prius motor and the proposed multi-layer IPM motors are tabulated in Table 4. It can be observed that by adding the flux barrier numbers, the generated reluctance components are enhanced.

4.2.2 Torque pulsation harmonic spectrum of the IPM models

The rated torque waveform of the 2004 Prius motor, and the optimal two-, three-, four-, and five-layer rotor structures are shown in Fig. 12. As tabulated in Table 5, a suppression of torque ripple from 26% to 10.98% is achieved when the optimal double-layer model is adopted. In addition, by adopting the optimal three-layer model, the torque pulsation is decreased from 26% to 6.4%. It can be

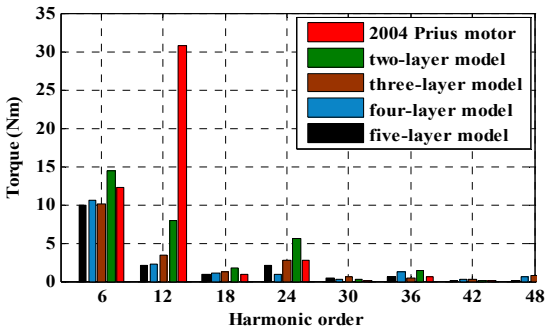

Fig. 13. Torque pulsation harmonics comparison of the representative IPM models (optimized asymmetric models)

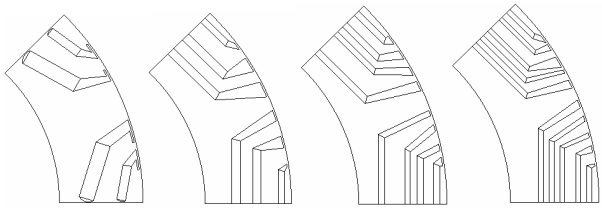

Fig. 14. Magnified views of the flux barriers of the multi-layer rotor structures (optimized asymmetric models)

seen that by increasing the number of flux barrier layers above three layers, the average torque and the torque pulsation are almost unchanged. L_d, L_q and ψ_{PM}-the PM flux linkage-for the proposed IPM structures are also given in Table 5. It should be noted that the d- and q-axis inductances considering the saturation, are obtained by the method proposed in [16] and the PM flux linkage is calculated based on FEM. In Table 5, it is observed that while the maximum value of the magnet volume is kept fixed for all five designs, the increase of the number of flux barrier layers almost increases the saliency ratio and the PM flux linkage. Therefore, the air-gap flux density and the developed torque are also improved.

Harmonic content of torque pulsation of the proposed

models at rated operating point under MTPA control (i.e., Fig. 12) is illustrated in Fig. 13. The torque harmonics, which are multiples of 6 as the dominant harmonics existing in the spectrum of torque waveforms, are taken into account for comparison. Furthermore, in the case of an 8-pole 48-slot 3-phase motor, due to an even number of slots per pole pairs (48/4=12), the torque pulsation harmonic at the order of such number is dominant [17]. This is effectively suppressed when the optimal five-layer structure is applied. The magnified views of the flux barriers of the optimal multi-layer rotor structures are shown in Fig. 14. It is obvious that the flux barrier end angles in the adjacent poles are different; therefore, the whole structure is asymmetric. It is also interesting to point out that there has been previously proposed an asymmetrical configuration for the rotor magnetic poles, that is called Machaon structure [18].

For the purpose of studying the effect of the current on torque ripple behavior, the five-layer rotor structure is taken into account. The FE analysis is performed with six current values along the MTPA trajectory: $0.25I_n$, $0.5I_n$, $0.75I_n$, I_n, $1.25I_n$ and $1.5I_n$. The torque versus time for different current values is shown in Fig. 15. In order to compare the torque ripple in different cases more obviously, the values of the torque corresponding to different current values-except I_n- are multiplied by the scaling factors. Some results comparing average torque and torque ripple for different current amplitudes are tabulated in Table 6.

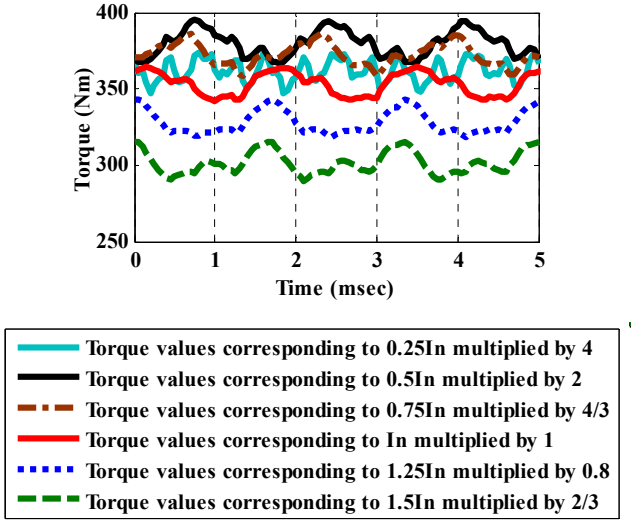

Fig. 15. Electromagnetic torque for different current values along the MTPA trajectory

Table 6. Torque comparison at different currents for five-layer model

Item	Average torque (Nm)	Torque pulsation at rated torque (%)
$0.25I_n$	90.492	7.43
$0.5I_n$	189.972	7.53
$0.75I_n$	279.278	7.48
I_n	353.37	6.32
$1.25I_n$	409.958	7.64
$1.5I_n$	452.37	8.47

4.2.3 Asymmetric flux barrier effect on torque ripple

A reduction of the torque ripple in IPM motors can be achieved by Adopting "Machaon" rotor structure, formed by different flux barrier geometries in adjacent poles [18]. When the geometry of the flux barriers is different in adjacent poles, a sort of compensation of the torque ripple harmonics is achieved [18]. The rated torque waveforms of the five-layer IPM motor, according to a rotor equipped with symmetric flux barrier geometries (A-type and B-type) and a rotor with asymmetric flux barrier geometries-a Machaon-type rotor-are compared in Fig. 17. Their geometries are shown in Fig.16. As observed, the torque ripple is evidently reduced by combining the effects of two symmetric flux barrier geometries.

The harmonic contents of torque pulsation for the above geometries are illustrated in Fig.18. The torque harmonics of 12th and 24th order (corresponding to the first and second slot harmonic) are high for A-type and B-type rotor structures. On the contrary, the torque harmonics of such orders in asymmetric rotor structure are drastically reduced.

To explain this result, by comparing the torque harmonics

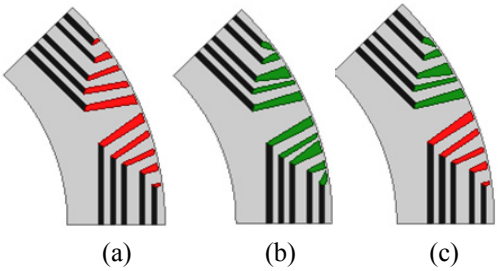

Fig. 16. Geometries of (a) symmetric five-layer model (A-type), (b) symmetric five-layer model (B-type) and (c) Asymmetric five-layer model

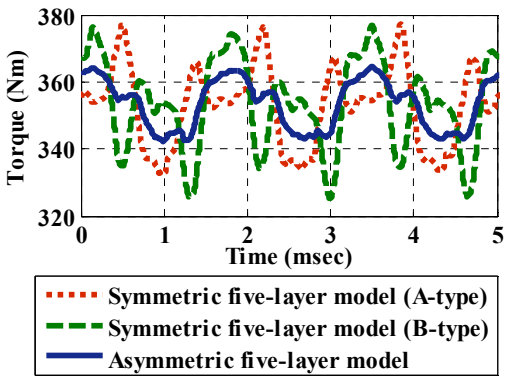

Fig. 17. Electromagnetic torque at rated condition for symmetric and asymmetric five-layer rotor structures

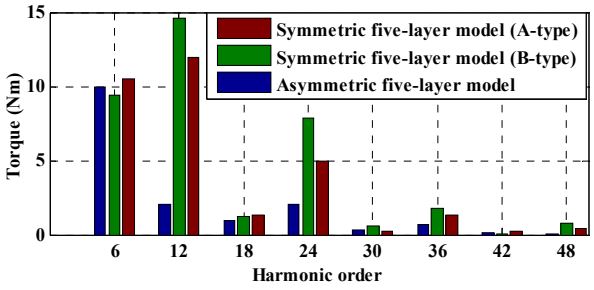

Fig. 18. Torque pulsation harmonics comparison of symmetric and asymmetric five-layer models

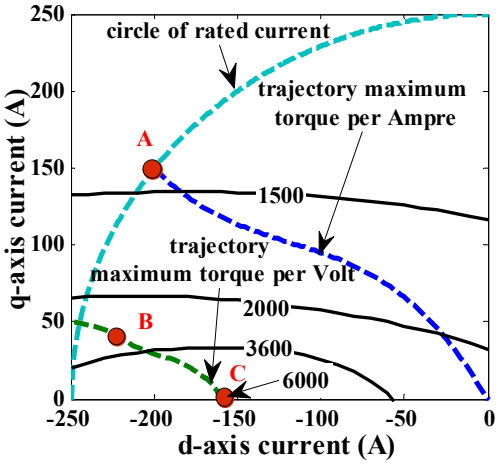

Fig. 19. Operation points of the five-layer model in the Id-Iq coordinate system

of these orders for the above geometries, it can be seen that the torque harmonic of such orders for symmetric A-type and B-type motors are out of phase of almost 180 degrees. As a result, the adoption of the Machaon-type rotor with combining two symmetric rotor structures allows a reduction of torque ripple harmonics.

4.2.4 Flux weakening performance

The typical operating capabilities of the optimal five-layer IPM model including the torque-speed and power-speed curves are illustrated in Fig. 20. Theses curves are determined by the parameters of the motor as well as the limits on the voltage and current from the motor drive system [21]. Inspection of Fig.20.a indicates that the optimized five-layer IPM motor can exhibit more torque than that of 2004 Prius motor at the constant torque range. While the Prius motor has a higher field weakening index-which is defined as the ratio of the rated current to the machine characteristic current-and as a consequence, it has a greater field weakening region.

In Fig. 19, the operating point A, which refers to the base point of the application, is reached when the machine operates along the MTPA trajectory. When the motor operates below the base speed, the drive operating region is

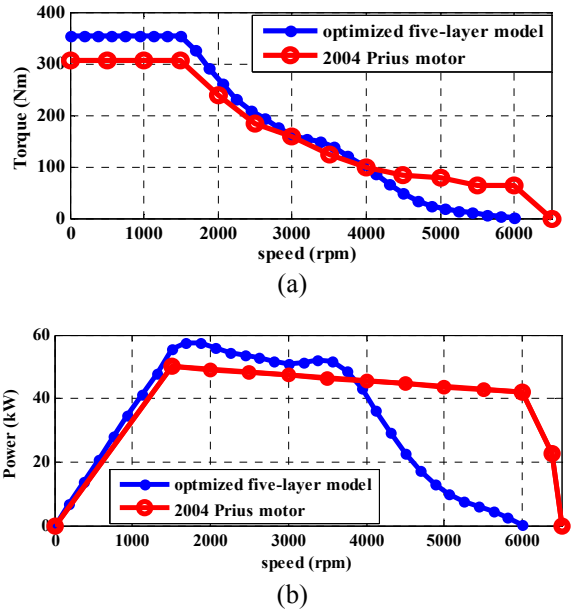

Fig. 20. (a) Torque-speed and (b) power-speed characteristics (for rated current) for the optimized five-layer model and 2004 Prius motor

Table 7. Withstand d-axis current for the IPM motors

Item	2004 Prius IPM	Two-Layer IPM	Three-layer IPM	Four-layer IPM	Five-layer IPM
d-axis current	$0.85I_{max}$	$0.98I_{max}$	$1.05I_{max}$	$2.1I_{max}$	$1.87I_{max}$

referred to as the MTPA to achieve the constant torque control operation, where the maximum torque is limited by the rated stator current. The operating point B, which is located on the maximum torque-per-volt (MTPV) trajectory, is reached when the motor is controlled by the flux weakening (FW) method. The current vector moves along such locus up to the point C, the speed of which is theoretically infinite and the torque of which is zero.

4.3 Evaluation of irreversible demagnetization of magnets in IPM motors

According to [19], a negative d-axis stator current is generally recognized to be a primary source of demagnetizing MMF. Moreover, as noted earlier, when the maximum current is applied to the stator winding and the maximum torque is produced, maximum negative d-axis current value flows in the opposite direction of the PM's MMF; therefore, the aforementioned working point is considered as the worst-case study in this paper. For the demagnetization analysis of PMs, the maximum coercive force of each PM should be calculated according to the rotating angle. The waveforms of maximum coercive force distribution in each PM of five-layer model are shown in Fig. 22. In addition, the flux density distribution contours of the optimized five-layer model are shown in Fig. 23. The results for two-,

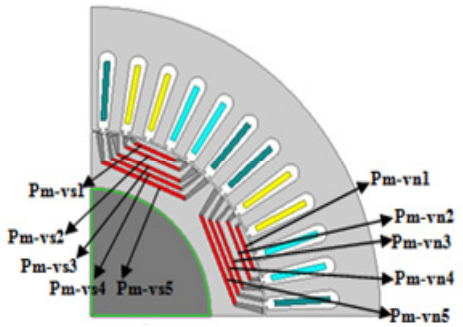

Fig. 21. The notations of segment PMs of optimal five-layer flat-type IPM

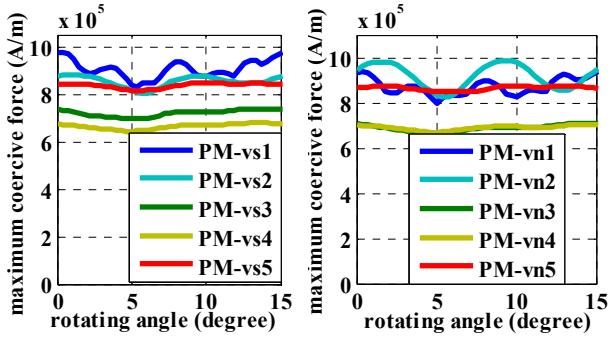

Fig. 22. Maximum coercive force distribution of each PMs of optimal five-layer flat-type IPM versus rotor position

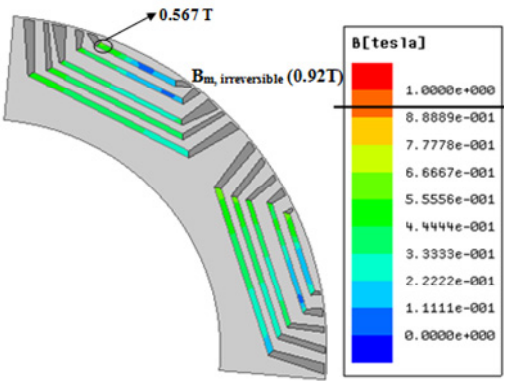

Fig. 23. Flux density distribution contours for optimized five-layer flat-type IPM motor when the maximum current is applied to the stator windings and the maximum output torque is produced

three-, and four-layer machines are calculated and are available, but, because of limited number of pages, they are not brought in this paper. The notations of segment PMs forming the poles of five-layer structure is represented in Fig. 21. It is clear that the flux barrier shapes and the PM dimensions are properly designed in a manner that the introduced models have the reliable characteristics on the demagnetization.

For the purpose of comparing the rotor structures of this study from the irreversible demagnetization point of view, the negative d-axis current-the current component most responsible for demagnetization-is increased to the value, at which the PMs undergo irreversible demagnetization. Table 7 summarizes the maximum withstand amplitude of the d-axis current for the rotor structures. It is obvious that by increasing the flux barrier layers, the maximum withstand amplitude of the d-axis current increases. It can be said that the reluctances of the flux barrier ends and ribs get smaller due to increasing the area of them, so, the demagnetization flux of the four-layer IPM easily flows along the rib of the flux barriers, compared to the 2004 Prius motor.

5. Conclusion

The shape of flux barriers, magnet dimensions and the positions of magnet layers have substantial effect on demagnetization characteristics in multi-layer IPM machines. In this paper, the 2004 Prius motor is considered as the baseline machine, and four types of IPM machines with asymmetric patterns of flux barriers (v-type two-layer and flat-type three-, four- and five-layer structures) are introduced and developed for optimization through a multi-objective design optimization based on the GA. The optimization process aims to improve the rated torque performance without additional PM volume increase and robustness against irreversible demagnetization (preventing irreversible demagnetization of PMs). Comparing to the reference machine, by applying the proposed optimal two- and three-layer structures, the rated main torque can be increased by 5% and 14% and the rated torque pulsation can be reduced from 26% to 10.98% and 6.4%, respectively. In addition, the IPM machines with optimum four- and five-layer flux barriers in the rotor have almost the same torque characteristics compared to the machine with three-layer flux barriers in the rotor. From the irreversible demagnetization point of view, the introduced rotor structures are evaluated by FEM at severe conditions of temperature and applied stator current.

References

[1] R. H. Staunton, T. A. Burress, and L. D. Marlino, "Evaluation of 2005 Honda Accord hybrid electric drive system," Oak Ridge Nat. Lab, Oak Ridge, TN, USA, Rep. ORNL/TM-2006/535, 2006.

[2] K. T. Chau, C. C. Chan, C. Liu, "Overview of Permanent-Magnet Brushless Drives for Electric and Hybrid Electric Vehicles," *IEEE Trans. on Industrial Electronics*, vol. 55, pp. 2246-2257, June, 2008.

[3] N. Bianchi and T. M. Jahns, Design, Analysis, and Control of Interior PM Synchronous Machines. Piscataway, NJ: IEEE, Oct. 2004, *IEEE Ind. Appl.*

Soc. Elect. Mach. Committee.

[4] J. M. Miller, Propulsion System for Hybrid Vehicles, ser. Inst. Elect.Eng. Power Energy 45. London, U.K.: IEE, 2004.

[5] K. J. Lee, K. C. Kim, S. Kim, J. S. Ahn, S. Y. Lim, and J. Lee, "Optimal Magnet Shape to Improve Torque Characteristics of IPMSM," *J. Appl. Phys*., vol. 97, p. 10Q505, 2005.

[6] K. C. Kim, S. B. Lim, D. H. Koo and J. Lee, "The Shape Optimization of Permanent Magnet for Permanent Magnet Synchronous Motor Considering Partial Demagnetization", *IEEE Trans. Magn*., vol. 42, no. 10, pp. 3485-3487, 2006

[7] N. Bianchi, M. Degano and E. Fornasiero "Sensitivity Analysis of Torque Ripple Reduction of Synchronous Reluctance and Interior PM motors", *Proc. IEEE ECCE*, pp. 1842-1849, 2013.

[8] S. Morimoto, S. Ooi, Y. Inoue, and M. Sanada, "Experimental Evaluation of a Rare-Earth-Free PMASynRM With Ferrite Magnets for Automotive Applications," *IEEE Transactions on Industrial Electronics*., vol. 61, no. 10, pp. 5749-5756, Oct. 2014.

[9] Z. Q. Zhu, D. Ishak, D. Howe, and C. Jintao, "Unbalanced Magnetic Forces in Permanent-Magnet Brushless Machines With Diametrically Asymmetric Phase Windings," *Industry Applications, IEEE Transactions on*, vol. 43, pp. 1544-1553, 2007.

[10] S. Morimoto, S. Ooi, Y. Inoue, and M. Sanada, "The Shape Design of Permanent Magnet for Permanent Magnet Synchronous Motor Considering Partial Demagnetization," *IEEE Trans. Magn*., vol. 42, no. 10, pp. 3485-3487, Mar. 2006.

[11] S. Ruoho, J. Kolehmainen, J. Ikaheimo, and A. Arkkio, "Interdependence of Demagnetization, Loading, and Temperature Rise in a PM Synchronous Motor," *IEEE Trans. Magn*., vol. 46, no. 3, pp. 949-953, Mar. 2010.

[12] J. S. Hsu, C. W. Ayers, and C. L. Coomer, "Report on Toyota/Prius Motor Design and Manufacturing Assessment," Oak Ridge Nat. Lab., Oak Ridge, TN, USA, Rep. ORNL/TM-2004/137, 2004.

[13] J. S. Hsu, C. W. Ayers, and C. L. Coomer, "Reprot on Toyota/Prius Motor Torque Capability, Torque Property, No-load Back Emf, and Mechanical Losses," Oak Ridge Nat. Lab., Oak Ridge, TN, USA, Rep. ORNL/TM-2004/137, 2004.

[14] F. Fulginei and A. Salvini, "Comparative Analysis Between Modern Heuristics and Hybrid Algorithms," *Int. J. Comput. Math. Electr. Electron. Eng*., vol. 26, no. 2, pp. 259-268, 2007.

[15] H. Huang, Y. Hu, Y.Xiao, and H. Lyu, "Research of Parameters and Antidemagnetization of Rare-Earth-Less Permanent Magnet-Assisted Synchronous Reluctance Motor," *IEEE Trans. Magn*., vol. 51, no. 11, Nov. 2015.

[16] S.-I. Kim, G.-H. Lee, J.-P. Hong, and T.-U. Jung, "Design Process of Interior PM Synchronous Motor for 42-V Electric Air-Conditioner System in Hybrid Electric Vehicle," *IEEE Trans. Magn*., vol. 44, no. 6, pp. 1590-1593, Jun. 2008.

[17] Seok-Hee Han; Jahns, T.M.; Zhu, Z.Q., "Design Tradeoffs Between Stator Core Loss and Torque Ripple in IPM Machines," *Industry Applications*, *IEEE Transactions on*, vol. 46, no. 1, pp. 187-195, Jan.- Feb. 2010.

[18] P. Alotto, M. Barcaro, N. Bianchi, and M. Guarnieri, "Optimization of Interior PM Motors with Machaon Rotor Flux Barriers," *IEEE Trans. Magn*., vol. 47, no. 5, pp. 958-961, May, 2011.

[19] Choi, Gilsu, and T. M. Jahns. "Demagnetization Characteristics of Permanent Magnet Synchronous Machines," *In Industrial Electronics Society, IECON 2014-40th Annual Conference of the IEEE*, pp. 469-475, IEEE, 2014.

[20] J. S. Hsu, C. W. Ayers, C. L. Coomer, R. H. Wiles, "Report on Toyota/Prius Motor Torque Capability, Torque Property, No-Load Back EMF, and Mechanical Losses," Oak Ridge National Laboratory, Rep. ORNL/TM- 2004/185, Sep. 2004.

[21] T. Jahns, "Flux-weakening regime operation of an interior permanent-magnet synchronous motor drive," *IEEE Transactions on Industry Applications*, vol. IA-23, no. 4, pp. 681-689, July, 1987.

M. S. Mirazimi was born in Isfahan, Iran, in 1987. She received the B.Sc. degree from University of Yazd, Yazd, Iran, in 2010 and the M.Sc. degree in 2012 from University of Tabriz, Tabriz, Iran. She is currently working toward the Ph.D. degree at the Department of Electrical Engineering at the University of Isfahan. Her current research interests have included application of time-stepping finite element analysis in electromagnetic and electrical machines, and design and optimization of permanent-magnet synchronous machines.

A. Kiyoumarsi was born in Shahr-e-Kord, Iran, in 1972. He received B.Sc. (with honors) from Petroleum University of Technology (PUT), Ahwaz, Iran, in electronics engineering in 1995. He also received M.Sc. (with the second best rank) and Ph.D. degrees (with the second best rank), from Isfahan University of Technology (IUT), Isfahan, Iran, in electrical power engineering in 1998 and 2004, respectively. In 2005 he joined the University of Isfahan as an

assistant professor of electrical machines. He was a Post-Doc. Research fellow of the Alexander-von-Humboldt foundation at the Institute of Electrical Machines, Technical University of Berlin, in 2006 and 2007. He was also a visiting guest professor at the Institute of Electrical Machines (IEM), RWTH, Aachen University, in July 2014. In 2012, he became an associate professor of electrical machines. His research interests have included application of time-stepping finite element analysis in electromagnetic and electrical machines, and design and analysis of interior permanent-magnet synchronous motor-drive.

Sayed M. Madani received the B.Sc. degree from Sharif University of Technology, Tehran, Iran, in 1989, the M.Sc. degree from the University of Tehran, Tehran, in 1991, and the Ph.D. degree from the Eindhoven University of Technology, Eindhoven, The Netherlands, in 1999, all in electrical power engineering. From 2000 to 2005, he worked with Texas A&M University, University of Puerto Rico, and University of Wisconsin at Madison, as an Assistant Professor or a Visiting Professor. From 2005 to 2011, he worked with Isfahan University of Technology as an Assistant Professor. He is currently an Associate Professor at University of Isfahan, Isfahan, Iran. His research interests include power system protection and electrical machine drives.